Neutron powder diffraction studies of sulfuric acid hydrates. II. The structure, thermal expansion, incompressibility, and polymorphism of sulfuric acid tetrahydrate ($D_2SO_4 \cdot 4D_2O$)

A. D. Fortes,[a] I. G. Wood, and L. Vočadlo
Department of Earth Sciences, University College London, Gower Street, London WC1E 6BT, United Kingdom

L. Chapon
ISIS Facility, Rutherford Appleton Laboratory, Chilton, Didcot, Oxfordshire OX11 0LA, United Kingdom

K. S. Knight
ISIS Facility, Rutherford Appleton Laboratory, Chilton, Didcot, Oxfordshire OX11 0LA, United Kingdom and The Natural History Museum, Cromwell Road, London SW7 5BD, United Kingdom

R. I. Smith
ISIS Facility, Rutherford Appleton Laboratory, Chilton, Didcot, Oxfordshire OX11 0LA, United Kingdom

(Received 4 October 2007; accepted 29 November 2007; published online 7 February 2008)

We report results of the first neutron powder diffraction study of sulfuric acid tetrahydrate (SAT); $D_2SO_4 \cdot 4D_2O$ is tetragonal, space group $P\bar{4}2_1c$, with two formula units per unit cell. At 1.7 K the unit-cell dimensions are $a=b=7.475\,12(6)$ Å, $c=6.324\,66(5)$ Å and $V=353.405(5)$ Å^3. At 225 K the unit-cell dimensions are $a=b=7.4833(1)$ Å, $c=6.4103(1)$ Å, and $V=358.98(1)$ Å^3. The deuteron positions refined from the neutron data are in excellent agreement with the single crystal x-ray analysis of Kjällman and Olovsson [Acta Crystallogr., Sect. B: Struct. Crystallogr. Cryst. Chem. **B28**, 1692 (1972)]; the structure consists of SO_4^{2-} and $D_5O_2^+$ ions hydrogen bonded to form a three dimensional network. Although no structural change is observed between 2 K and the melting point at ~232 K, the thermal expansion and incompressibility of the crystal are highly anisotropic. The bulk modulus of SAT at 200 K is 9.2(2) GPa, $(\partial K/\partial P)_T=7.9(8)$, and $-(\partial K/\partial T)_P=10.6(5)$ MPa K^{-1}, values which are very similar to D_2O ice Ih. A new polymorph of SAT has been discovered above 235 K at 5.5 kbars. The structure of this phase could not be determined, but we have indexed the diffraction pattern with a monoclinic unit cell of likely space-group $P2_1/a$ ($Z=2$). SAT-II has a lower density than SAT-I under the same P/T conditions; the refined unit-cell parameters at 235 K, 5.435 kbars are $a=6.1902(3)$ Å, $b=11.1234(5)$ Å, $c=5.6446(3)$ Å, $\beta=110.287(4)°$, and $V=364.56(2)$ Å^3. This phase has been quenched to low pressures and temperatures, and we have obtained estimates of the thermal expansivity and incompressibility which reveal SAT-II to be significantly stiffer and more isotropic than SAT-I. © *2008 American Institute of Physics*. [DOI: 10.1063/1.2827474]

I. INTRODUCTION

The sulfuric acid-water system (Fig. 1) represents a model system for understanding the crystal chemistry of a diverse range of related structures ($H_2SO_4 \cdot xH_2O$, with $x=0$, 1, 2, 3, 4, 6.5, and 8),[1] including a number of high-pressure polymorphs.[2,3] The system also has an impact on the global climate, being responsible for the formation of aerosols in the terrestrial stratosphere.[4,5] Sulfuric acid tetrahydrate (SAT) is thought to be particularly important because of its role in promoting the nucleation of stratospheric ice clouds,[6,7] controlling the heat balance in the upper atmosphere. Sulfuric acid hydrates, and hydrates of sulfate salts, have been identified on the surface of Jupiter's moons Europa and Ganymede using near infrared spectroscopy;[8–10] these may be derived from an acidic subsurface ocean[11,12] or by implantation of sulfur ions originating from neighboring Io.[13] As part of our broader study of sulfuric acid hydrates,[14] we have carried out a series of neutron diffraction measurements upon perdeuterated SAT at the ISIS pulsed spallation neutron source, Rutherford Appleton Laboratory, measuring diffraction patterns at a wide range of temperatures (liquid helium to SAT melting) and hydrostatic pressures up to 5.5 kbars.

The structure of SAT was solved by Kjällman and Olovsson[15] from single crystal x-ray diffraction of $H_2SO_4 \cdot 4H_2O$ and $D_2SO_4 \cdot 4D_2O$, the positions of the hydrogen (deuterium) atoms being assigned on the basis of chemical arguments and weak peaks in Fourier difference maps. Thus it is of interest to confirm the positions of the H(D) atoms in SAT using neutron diffraction. Furthermore, since it is important to be able to model surface interactions between SAT condensates and water molecules, an appreciation of the behavior of the crystal at stratospheric temperatures

[a]Author to whom correspondence should be addressed. Electronic mail: andrew.fortes@ucl.ac.uk.

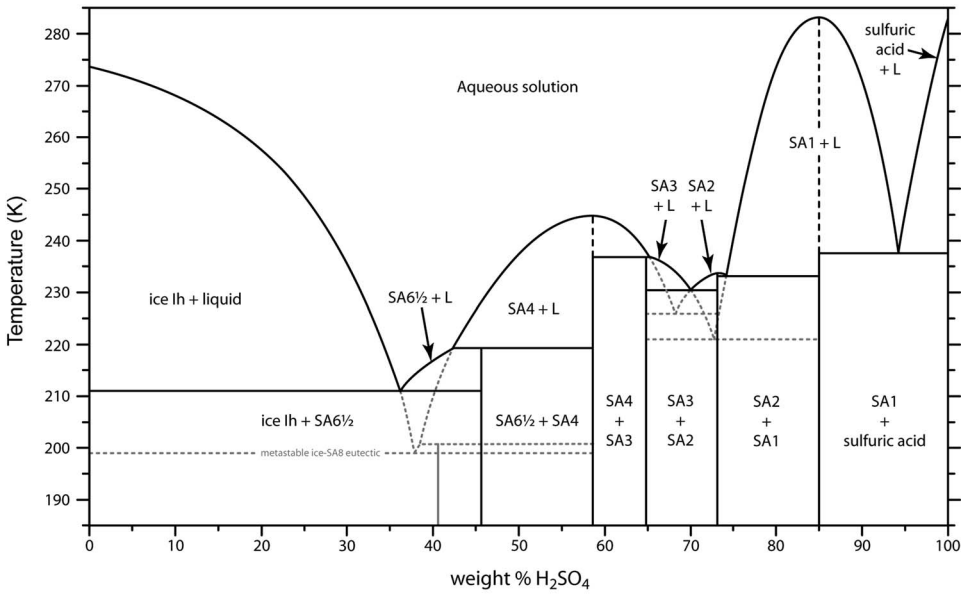

FIG. 1. The binary system $H_2O-H_2SO_4$, illustrating the place of sulfuric acid tetrahydrate (SA4) amongst the many other hydrates. Redrawn after Beyer *et al.* (Ref. 1), and references therein. Dashed gray lines represent metastable phase boundaries. SA*x* labels indicate the phases $H_2SO_4 \cdot xH_2O$.

(150–250 K) is critical. Calculations depend on robust interatomic potentials that are able to reproduce the thermoelastic properties of SAT, and accurate crystallographic measurements underpin the fitting of such potentials.

The most suitable method for achieving these objectives is powder neutron diffraction. Given the large incoherent scattering length of the hydrogen atom, we use a perdeuterated analog in order to achieve good signal to noise ratio in the measured diffraction data (See Ref. 16). Time-of-flight neutron powder diffraction measurements were made on three different diffractometers at ISIS: POLARIS, GEM, and the high resolution powder diffractometer (HRPD). Both POLARIS (Ref. 17) and GEM (Ref. 18) are high flux, medium resolution instruments, the latter having the advantage of large detector solid angle coverage (and a slightly different incident neutron spectrum by virtue of viewing another moderator), which allows for very rapid data collection out to long *d* spacings even in strongly absorbing sample environments, such as a TiZr high-pressure gas cell. HRPD (Ref. 19) is ideally suited to very accurate determination of cell parameters by virtue of its long target-to-specimen flight path (95 m), yielding a resolution ($\Delta d/d$) of 4×10^{-4} in the backscattering detectors.

We describe the details of the data acquisition in each of the three experiments (summarized in Table I), and the treatment of the data, in Sec. II. In Sec. III, we discuss the crystal structure refinements (Sec. III A), the thermal expansivity at room pressure and at 5.5 kbars (Secs. III B and III C), the incompressibility (Sec. III D), and the thermoelastic cross terms (Sec. III E). In Sec. III F, we describe the newly discovered high-pressure polymorph, SAT-II, and estimate its thermoelastic properties.

II. EXPERIMENTAL METHOD

Reagent grade D_2SO_4 (Aldrich Chemical Co., 98 wt % D_2SO_4, 99 at. % D) was diluted with D_2O (Aldrich Chemical Co., 99 at. % D) to form a solution with the requisite stoichiometry (1:4). However, for the third experiment described below (Sec. III C), our intention was to form sulfuric acid trihydrate (SATri), so the solution prepared was in the molar ratio 1:3. Since this sample crystallized SAT rather than SATri, we report the results here, although the presence of nearly 50 mol % of D_2SO_4-rich glass in the specimen resulted in severe crystallographic strain on the SAT component.

The existing literature reports the propensity of sulfuric acid solutions to supercool, and form glasses when cooled rapidly; indeed Kjällman and Olovsson[15] report that the deuterated analog is even more disposed to such behavior. We attempted initially to flash-freeze our solutions in a liquid-nitrogen-cooled mortar and then grind them to a fine powder. However, even at nitrogen temperatures, we discovered that the solution formed a toffeelike mass which defied grinding. Subsequent tests revealed that we could prepare crystalline SAT by first flash freezing the solution to 100 K, at which

TABLE I. Summary of the properties of sulfuric acid tetrahydrate obtained in each of the three neutron powder diffraction experiments described in Sec. II.

POLARIS
SAT-I thermal expansivity at 1 bar
SAT-I crystal structure refinements at 1.7, 75, 150, and 225 K (at 1 bar)
SAT-I melting at ~232 K (at 1 bar)
GEM
SAT-I incompressibility at T=200 K
SAT-I crystal structure refinement at 200 K, 3950 bars
SAT-I thermal expansivity at 5.5 kbars
SAT-I melting at ~245 K, 2760 bars
SAT-I → SAT-II transformation at 230 K, 5470 kbars
SAT-II unit cell at 235 K 5455 bars, 200 K 5450 bars, 50 K 5435 bars, 70 K 125 bars, and 205 K 2750 bars
HRPD
SAT-I crystal structure refinement at 217 K (at 1 bar)

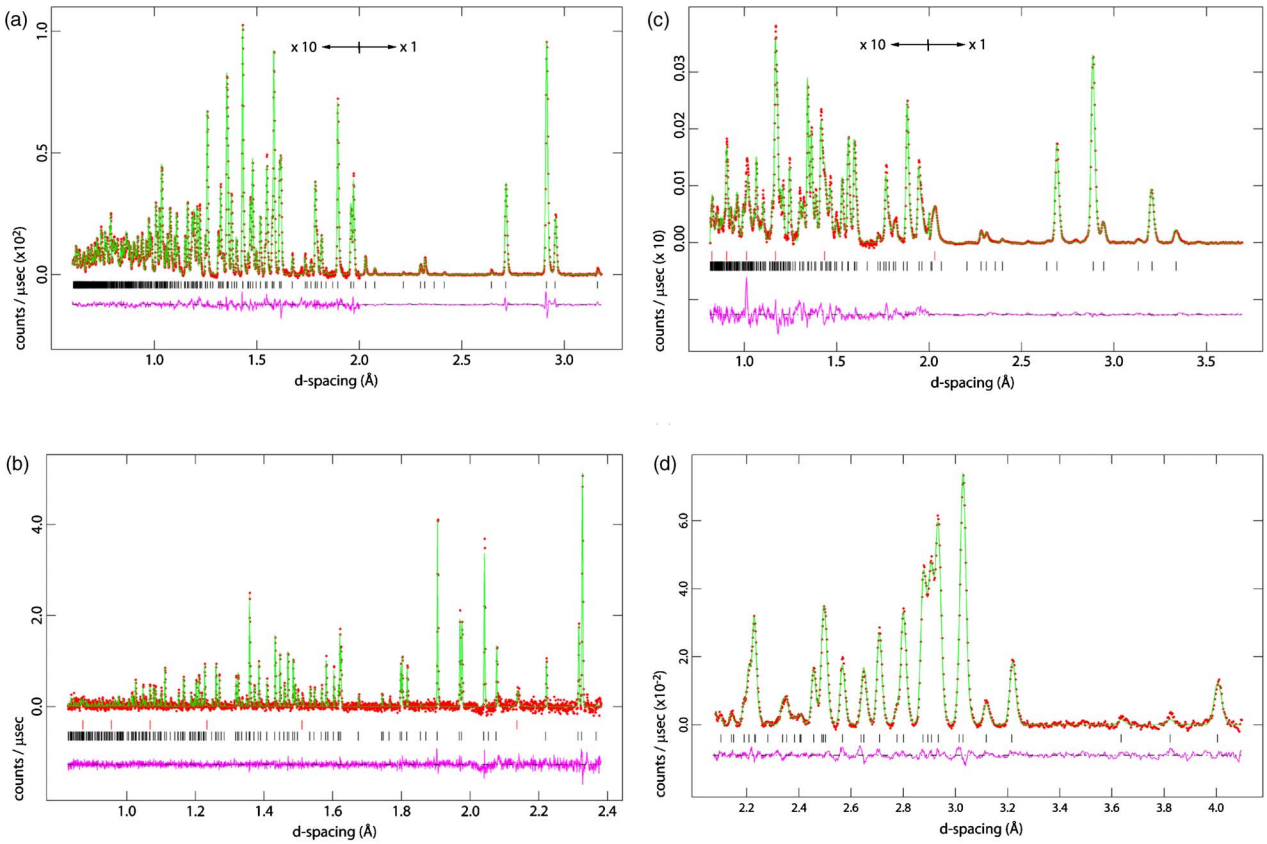

FIG. 2. (Color online) (a) Diffraction pattern collected in the backscattering detectors of POLARIS at 1.7 K. Note the change in scale below d=2.0 Å. (b) Diffraction pattern collected in the backscattering detectors of HRPD at 217 K. The upper set of tick marks shows the positions of Bragg reflections from vanadium, and the lower set from the specimen. (c) Diffraction pattern collected in bank 4 of GEM (2θ=63.62°) at 200 K, ~3970 bars. The upper set of tick marks shows the positions of Bragg reflections from steel, and the lower set are from the specimen. Note the change in scale below d=2.0 Å. (d) Diffraction pattern of SAT-II collected in bank 4 of GEM (2θ=63.62°) at 50 K, 5435 bars. The solid line is a LeBail profile refinement using the $P2_1/a$ cell obtained by indexing in DICVOL (cell parameters given in Table V).

point a glass formed, and then warming the sample to ~200 K; both steps being carried out in the cryostat prior to mounting on the beamline.

A. The ambient-pressure, variable temperature POLARIS experiment

An aluminum-framed slab can, having internal dimensions 10 mm (w)×10 mm (d)×40 mm (h), with vanadium windows (sealed with indium wire) was loaded with 6.34 g of solution and approximately 0.1 g of silica wool to aid the crystallization of a randomly oriented polycrystalline mass. Gadolinium foil shielding was screwed over the front face of the aluminum body of the can, which was then lowered rapidly into a Dewar of liquid nitrogen and subsequently transferred into a Dewar of dry ice (at 195 K) for ~12 h. Following this, the sample can was attached to the cryostat center stick and a small electric heater and a RhFe temperature sensor inserted into holes drilled in the aluminum frame of the sample can to facilitate accurate measurement and control of the sample temperature—the sample can remaining immersed in a bath of liquid nitrogen throughout the procedure. Finally, the center stick assembly was loaded into a helium flow "Orange" cryostat (AS Scientific, Abingdon, UK), which had been precooled to 100 K, and allowed to anneal for a further 20 h before being mounted on the POLARIS beamline. Preliminary inspection of a diffraction pattern collected from the solid specimen at 100 K showed that SAT had crystallized, so the temperature was reduced to 1.7 K and a low-noise diffraction pattern (150 μA h) was collected. Diffraction patterns were then acquired upon warming, in 4 K intervals from 6 to 230 K, with an additional diffraction pattern collected at 232 K, counting for ~10 min (30 μA h) at each temperature with 5 min of warming and thermal equilibration between each datum. The absence of Bragg peaks in the diffraction pattern collected at 232 K indicated that the sample had melted (indeed the 230 K diffraction pattern showed evidence of the onset of melting), which is in agreement with the approximate melting temperature of the deuterated isotopomer, 234 K, found by Kjällman and Olovsson:[15] note that the hydrogenous isotopomer melts at 244.9 K.[20] The sample temperature was immediately reduced to 220 K, which caused the specimen to recrystallize promptly; diffraction data were then collected at 220 K for 42 μA h. Finally, longer runs with good counting statistics, suitable for full structure refinement, were collected from the recrystallized sample at 225 K (165 μA h), 150 K (150 μA h), and 75 K (365 μA h); see Fig. 2(a).

B. The high-pressure GEM experiment

A cylindrical pressure cell (sample dimensions; 7 mm diameter×40 mm high; 10.5 mm wall thickness; and

constructed from a "null scattering" TiZr alloy) was loaded with 1.8 cm^3 of solution and approximately 0.1 g of silica wool. The cell was mounted to a center stick and sealed under 150 bars of helium gas pressure. Copper collars fitted with cartridge heaters and RhFe temperature sensors were attached to the top and bottom of the TiZr cell for accurate measurement and control of the sample temperature prior to loading into an Orange cryostat on the GEM beamline. Hydrostatic pressure in the system was generated and maintained using a helium gas intensifier (Stansted Fluid Power, Stansted, Essex, UK). Initial inspection of a diffraction pattern collected at 160 K showed that the specimen was an amorphous solid. Warming to 220 K caused the specimen to crystallize SAT; the pressure and temperature were stabilized at 115 bars, 200 K and a low-noise data set (170 μA h) was collected. Diffraction data were then collected upon pressurization with helium gas at 200 K, increasing the pressure in approximately 500 bar increments up to 5500 bars, counting for 23 μA h at each datum: at 5450 bars, 200 K, a further low-noise data set was collected (190 μA h); see Fig. 2(c). The temperature was then reduced to 50 K, which caused the pressure in the system to drop to 4275 bars; 23 μA h data sets were then collected upon repressurization in ~500 bar intervals from 4275 up to 5500 bars at 50 K. From 50 K, the sample was warmed in 5 K intervals, counting for 8 min (20 μA h) with 5 min of temperature equilibration at each point. During warming from 50 to 235 K, as the temperature of the gas in the system changed, the pressure was maintained at 5475 ± 115 bars automatically by the helium gas intensifier.

Upon reaching 230 K (at 5470 bars) the diffraction pattern changed, indicating either that the sample had disproportionated (into a lower hydrate plus a high-pressure ice polymorph) or had undergone a polymorphic phase change. Data were collected at 235 K (5455 bars) for 1 h (170 μA h), and then the specimen was cooled to 50 K; having failed to revert to the original SAT diffraction pattern, a 4 h data set (673 μA h) was collected at 50 K, 5435 bar (Fig. 2(d)). The specimen was then rapidly warmed to 200 K, the gas pressure was reduced to 2750 bars, and a series of short duration datasets (20 μA h per datum) were collected at 5 K intervals upon warming from 200 to 245 K at 2750 ± 10 bars. Regrowth of SAT-I crystals became evident at 215 K, with significant backtransformation being observed at 240 K: the sample was seen to be molten in diffraction data acquired at 245 K, 2760 bars. Immediate cooling of the sample to 230 K failed to induce crystallization, so the gas pressure was reduced to ~400 bars, and the temperature was reduced to 100 K; warming to 200 K at 400 bars subsequently resulted in the formation of SAT crystals. Finally, the newly crystallized SAT was compressed to 5500 bars at 200 K and then warmed to 240 K, where the diffraction pattern of the new phase was observed once more. This high-pressure specimen was cooled to 100 K, whereupon the gas pressure was reduced to 100 bars. No backtransformation was observed and so a low-noise data set (~350 μA h) was collected at 70 K, 125 bars.

C. The ambient-pressure HRPD experiment

For this experiment, the 1:3 D_2SO_4:D_2O solution was pipetted into a 12 mm diameter cylindrical vanadium can along with ~0.15 g of silica wool. The can was sealed, attached to a center stick, and then dipped in liquid nitrogen before the assembly was loaded into an Orange cryostat (precooled to 125 K) mounted on the HRPD beamline. Upon first inspection the sample was observed to be amorphous; subsequent warming to 210 K caused SAT to crystallize—the D_2SO_4-rich residue apparently remaining as a glass throughout the remainder of the experiment. The only Bragg peaks in the diffraction pattern are those due to SAT with very minor contributions from vanadium in the sample environment.

A low-noise data set (129 μA h) was collected in the backscattering ($2\theta = 168°$) and 90° banks of HRPD at 217 K (Fig. 2(b)). The sample was then cooled to 4.2 K and another low-noise data set was collected (263 μA h). During cooling, a series of much shorter runs were counted; 3.9 μA h from 144 to 133 K, 3.5 μA h from 100 to 90 K, and 3.1 μA h from 75 to 60 K.

D. Data analysis

The structure of the low-pressure phase SAT-I was refined by the Rietveld method using the general structure and analysis software package, GSAS,[21] starting from the structural model of Kjällman and Olovsson.[15] The agreement in the absolute unit-cell volumes between the three experiments is relatively poor compared to the precision of the individual experiments, and this is probably due to unavoidable differences in sample position from one loading to the next, as well as differences in the geometry and dimensions of the sample containers. The unit-cell volume found on POLARIS is 0.26% smaller than on HRPD at the same temperature, and the extrapolated zero-pressure volume on GEM is 0.14% smaller than the value obtained on POLARIS; compare these with the uncertainty of ~0.001%–0.003% in the unit-cell volumes found on HRPD and POLARIS. We have observed similar offsets between the lattice parameters of data collected on HRPD and POLARIS in previous experiments using these instruments.[22,23]

Comparison of the data sets revealed that the mixed SAT+glass specimen investigated on HRPD exhibited signs of strain (although the 217 K data set appears to be the least strained), probably due to differential thermal expansion of the two components. Similar anomalies in the lattice parameters obtained on POLARIS between 160 and 190 K are likely due to the devitrification of a very small amount of residual glass in the sample, although no discernible changes in the background of the diffraction pattern can be seen which might support this suggestion. Data in this range were omitted from the fitting procedures outlined in the following section.

Analysis of the GEM data showed that the pressure line had become blocked when the sample was compressed above 4 kbars at 200 K. This was probably due to freezing of helium in the capillary, which experiences much lower temperatures as it passes through the body of the cryostat

TABLE II. Results of Rietveld refinement of the $D_2SO_4 \cdot 4D_2O$ structure (SAT-I) using data collected on POLARIS at 1.7, 75, 150, and 225 K and on GEM at 200 K 3.95 kbars (in italics).

		Fitted		Minus background		
	N_{data}	wRp	Rp	wRp	Rp	χ^2
1.7 K	3331	1.46	2.82	2.06	3.80	2.550
75 K	3331	1.96	3.43	3.10	4.75	5.543
150 K	3331	1.83	3.16	3.00	4.12	3.781
225 K	3331	1.46	2.35	2.99	3.50	2.664
3.95 kbars *200* K	*1884*	*1.03*	*0.90*	*1.03*	*0.95*	*9.483*

	a (Å)	c (Å)	V (Å^3)
1.7 K	7.475 12(6)	6.324 66(5)	353.405(5)
75 K	7.477 31(7)	6.337 33(10)	354.321(7)
150 K	7.479 73(9)	6.368 00(11)	356.266(8)
225 K	7.483 28(10)	6.410 32(12)	358.975(10)
3.95 kbars *200* K	*7.437 1(3)*	*6.2457(1)*	*345.45(2)*

	x	y	z	U_{iso} ($\times 100$) Å^2
S	0	0	0	0.10(fixed)
				0.60(12)
				1.58(17)
				2.23(24)
				0.10(fixed)
O1	0.1361(2)	0.0888(2)	0.1322(2)	0.75(2)
	0.1367(2)	0.0861(2)	0.1330(3)	1.07(4)
	0.1354(3)	0.0867(3)	0.1348(4)	1.75(5)
	0.1342(4)	0.0861(4)	0.1356(5)	2.82(8)
	0.1354(4)	*0.0843(4)*	*0.1396(2)*	*0.9(1)*
O2	0.0584(2)	0.3491(2)	0.5781(2)	0.81(2)
	0.0583(2)	0.3491(2)	0.5796(3)	1.17(3)
	0.0561(3)	0.3503(3)	0.5842(4)	2.11(5)
	0.0565(4)	0.3505(4)	0.5877(5)	2.97(7)
	0.0642(13)	*0.3499(10)*	*0.5743(7)*	*0.9(1)*
D1	0.0064(2)	0.2671(2)	0.6823(2)	1.85(3)
	0.0055(2)	0.2686(2)	0.6835(3)	2.03(4)
	0.0054(3)	0.2673(3)	0.6867(4)	2.83(6)
	0.0062(4)	0.2669(3)	0.6876(5)	3.75(8)
	0.0017(14)	*0.2626(10)*	*0.6724(9)*	*3.6(2)*
D2	0.1897(2)	0.3515(2)	0.6026(2)	1.75(3)
	0.1897(2)	0.3520(2)	0.6034(3)	1.85(4)
	0.1883(3)	0.3525(3)	0.6038(4)	2.81(6)
	0.1886(4)	0.3525(4)	0.6056(4)	3.74(9)
	0.1910(13)	*0.3533(10)*	*0.6025(6)*	*3.4(2)*
D3	0	0.5	0.5856(3)	1.86(3)
			0.5902(5)	2.47(6)
			0.5940(6)	3.36(8)
			0.5971(8)	4.55(11)
			0.5800(11)	*2.4(2)*

TABLE II. (*Continued.*)

SO_4 polyhedron geometry			
S–O1	1.475(1)	∠O1–S–O1	108.75(4)°
	1.473(2)		109.1(1)°
	1.478(2)		109.7(1)°
	1.476(3)		110.3(1)°
	1.472(1)(*restrained*)		*110.53*(*5*)°
Tetrahedron volume	1.645(6) Å^3	∠O1–S–O1	110.92(8)°
	1.640(6) Å^3		110.2(5)°
	1.655(11) Å^3		108.9(1)°
	1.650(14) Å^3		107.8(3)°
	1.636(*14*) Å^3		*107.4*(*1*)°

Hydrogen bond geometry					
	O–D	D···O	O···O	∠O–D···O	∠ D–O–D
O2–D1···O1	0.980(2)	1.686(2)	2.665(2)	176.8(2)°	107.4(1)°
	0.976(2)	1.672(3)	2.647(2)	178.0(2)°	108.1(4)°
	0.977(3)	1.656(3)	2.632(3)	177.0(3)°	108.2(3)°
	0.971(4)	1.658(4)	2.628(4)	176.6(3)°	108.6(4)°
	1.007(8)	*1.638(7)*	*2.638(9)*	*177.0*(*8*)°	*111.0*(*9*)°
O2–D2···O1	0.994(2)	1.669(2)	2.662(2)	176.7(2)°	
	0.994(2)	1.689(2)	2.683(2)	177.2(2)°	
	0.997(3)	1.697(3)	2.693(3)	177.8(3)°	
	0.995(3)	1.700(4)	2.695(4)	177.5(3)°	
	0.960(7)	*1.689(12)*	*2.648 (9)*	*171.6*(*7*)°	
O2···D3···O2	1.211(1)	1.211(1)	2.419(2)	175.5(1)°	
	1.212(2)	1.212(2)	2.419(2)	173.6(1)°	
	1.197(2)	1.197(2)	2.392(3)	174.0(2)°	
	1.198(3)	1.198(3)	2.392(4)	174.2(2)°	
	1.215(7)	*1.215(7)*	*2.428(11)*	*176.6*(*8*)°	

Scissor angle, θ	47.7(1)°	Sulfate tilt, ω	33.12(2)°
	47.8(2)°		32.20(2)°
	48.9(2)°		32.63(3)°
	48.6(3)°		32.68(4)°
	43.7(6)°		*31.9*(*3*)°

where it is in the center of the annular liquid helium reservoir. Heaters were attached to both the main length of the cryostat center stick (inside which ran the pressure pipe) and to the small exposed section of pipe at the bottom of the center stick onto which the TiZr cell was mounted, but we failed to prevent freezing of the pressure medium while attempting to balance the warming of the capillary against the need to keep heat from leaking down the center stick into the pressure cell. This blockage was not detected until after the data were collected and fitted. The blockage persisted until partway through the warming sequence which means that data from 50 to 165 K had to be discarded. However, the new high-pressure phase formed after the blockage had cleared, and at the stated pressure of 5.5 kbars.

In all of the experiments, some preferred orientation was evident, this being most severe in the high-pressure measurements on GEM, and least severe in the ambient-pressure HRPD measurements. In all cases, texture was accommodated using the spherical harmonic model implemented in GSAS, refining terms to 16th order (24 coefficients). Full structural refinements were carried out using data collected at 1.7, 75, 150, and 225 K in the POLARIS backscattering detectors (average $2\theta=145°$); data collected at 217 K in the HRPD backscattering detectors (average $2\theta=168°$); and data collected at low and high pressures (nominally 112 and 5450 bars) at 200 K in GEM bank 4 (average $2\theta=63°$). In each case, we refined the SAT unit-cell parameters (a and c), atomic coordinates and isotropic temperature factors, scale factors, background coefficients (ten-term shifted Chebyshev polynomial), profile coefficients ($\sigma_1, \sigma_2, \gamma_1$), and the texture coefficients. On HRPD, vanadium was included as a second phase to fit weak additional Bragg peaks arising from the

TABLE III. Results of Rietveld refinement of the $D_2SO_4 \cdot 4D_2O$ structure (SAT-I) using data collected on HRPD at 217 K.

		Fitted		Minus background		
	N_{data}	wRp	Rp	wRp	Rp	χ^2
217 K	3520	2.42	2.07	2.87	2.63	1.169
		a (Å)		c (Å)		V (Å^3)
217 K		7.489 52(4)		6.410 19(7)		359.566(4)
		x	y	z	U_{aniso} (×100) Å^2	
S		0	0	0	U_{11}=2.6(9)	U_{12}=0
					U_{22}=2.6(9)	U_{13}=0
					U_{33}=5(2)	U_{23}=0
O1		0.1364(7)	0.0876(6)	0.1303(10)	U_{11}=3.3(3)	U_{12}=0.4(2)
					U_{22}=1.8(3)	U_{13}=−1.6(3)
					U_{33}=4.2(5)	U_{23}=−0.3(2)
O2		0.0545(9)	0.3461(11)	0.5852(11)	U_{11}=1.5(3)	U_{12}=−0.4(3)
					U_{22}=4.7(5)	U_{13}=0.2(3)
					U_{33}=3.0(4)	U_{23}=0.4(3)
D1		0.0047(8)	0.2651(8)	0.6896(11)	U_{11}=3.7(3)	U_{12}=−1.2(3)
					U_{22}=5.2(5)	U_{13}=1.0(3)
					U_{33}=5.3(5)	U_{23}=0.5(3)
D2		0.1871(9)	0.3502(7)	0.6044(9)	U_{11}=4.5(4)	U_{12}=0.2(3)
					U_{22}=4.3(4)	U_{13}=1.6(3)
					U_{33}=4.5(5)	U_{23}=0.2(3)
D3		0	0.5	0.5920(17)	U_{11}=4.2(5)	U_{12}=0.0(5)
					U_{22}=7.5(8)	U_{13}=0
					U_{33}=3.8(7)	U_{23}=0
		SO_4 polyhedron geometry				
S–O1		1.474(4)		∠ O1–S–O1		108.7(3)°
Tetrahedron volume		1.642(23) Å^3		∠O1–S–O1		111.0(6)°
		Hydrogen bond geometry				
		O–D	D···O	O···O	∠O–D···O	∠D–O–D
O2–D1···O1		0.977(7)	1.655(9)	2.632(9)	176.9(7)°	108.3(9)°
O2–D2···O1		1.001(6)	1.699(9)	2.699(9)	177.8(7)°	
O2···D3···O2		1.223(8)	1.223(8)	2.446(10)	175.9(11)	
Scissor angle, θ		51.0(7)°		Sulfate tilt, ω		32.71(4)°

cryostat tails and sample can. In addition, the low texture index of the HRPD data (1.06) and the high resolution allowed us to refine reliable anisotropic temperature factors.

The GEM data were not explicitly corrected for attenuation by the TiZr pressure vessel. Instead, the data at 200 K, 112 bars were fitted using the 225 K POLARIS structural model, refining an absorption correction in GSAS in addition to the texture coefficients. This provided the basis for fitting the high-pressure data; note, however, that the extreme preferred orientation (texture index >300) means that the structural model obtained may have limited value. Free refinement of the structure yielded S–O bond lengths which were rather too small (~1.45 Å). As the expected bulk modulus of the sulfate tetrahedron is of order 100 GPa, it was considered reasonable to place hard restraints on the length of the S–O bonds (1.475 ± 0.005 Å, with a weighting FACTR=100). This resulted in a marginally poorer fit, although the observed bond length/angle trends agree with ambient-pressure results.

III. RESULTS

The Rietveld powder statistics, refined unit-cell dimensions, atomic coordinates, isotropic temperature factors, and selected interatomic bond distances and angles are given in Table II for the POLARIS data collected between 1.7 and 225 K, and for the GEM data refined at high pressure. Although the latter was nominally collected at 5.45 kbars, the refined unit-cell dimensions indicate that, as a result of the blocked pressure line, the actual pressure was 3.95 kbars.

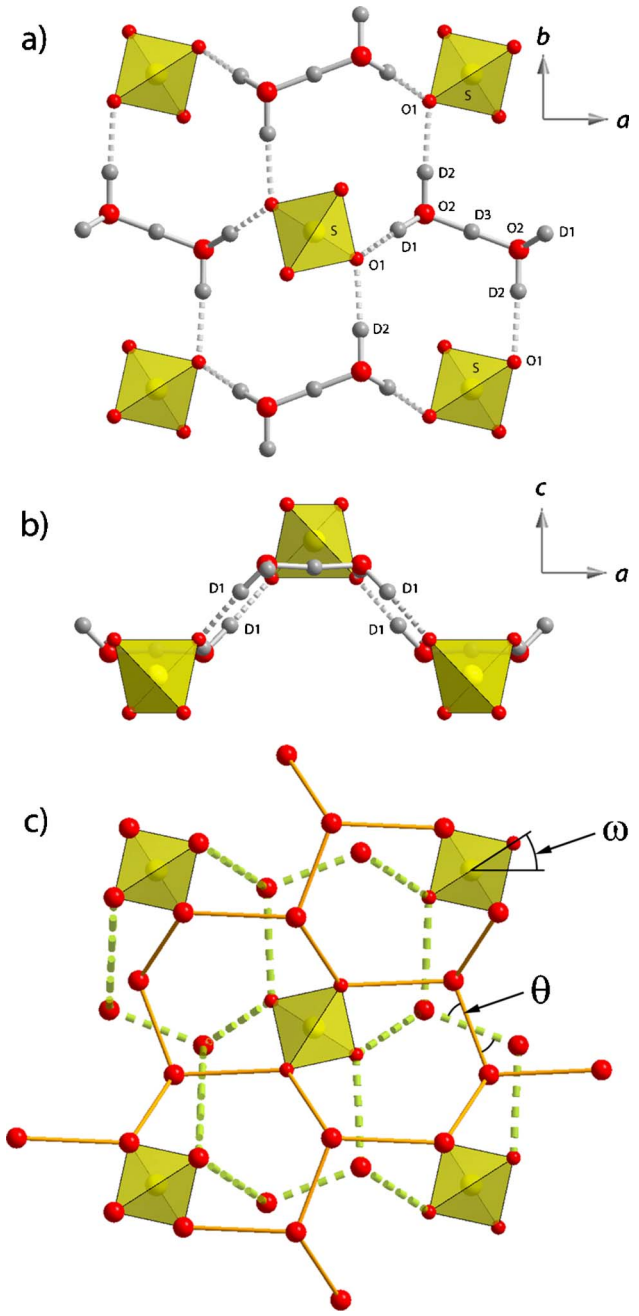

FIG. 3. (Color online) The structure of SAT-I; (a) viewed along the *c* axis, (b) perpendicular to the *c* axis, and (c) defining the angles θ and ω.

The structure refined from the 217 K HRPD data, with anisotropic temperature factors, is reported in Table III.

A. The crystal structure as a function of temperature

The main structural units of the low-pressure phase of SAT are sulfate ions (SO_4^{2-} tetrahedra) and diaquahydrogen ions ($D_5O_2^+$). In terms of the oxygen atoms, the structure consists of corrugated layers of hexagonal rings; the shared edges of each ring consist of four "normal" hydrogen bonds, one centered hydrogen bond (the spine of the $D_5O_2^+$ ion) and a short O–O contact across the edge of a sulfate ion [Figs. 3(a) and 3(b)]. These sheets are stacked perpendicular to the *c* axis, alternate sheets being related by the 2_1 screw axis [Fig. 3(c)]. For the purpose of understanding the minor structural changes as a function of pressure and temperature we define a "scissor" angle θ between the arms of alternate $D_5O_2^+$ ions along the *c* axis [Fig. 3(c)], and we also report the tilt angle ω made by the sulfate tetrahedra with the *a*-*c* plane [Fig. 3(c)].

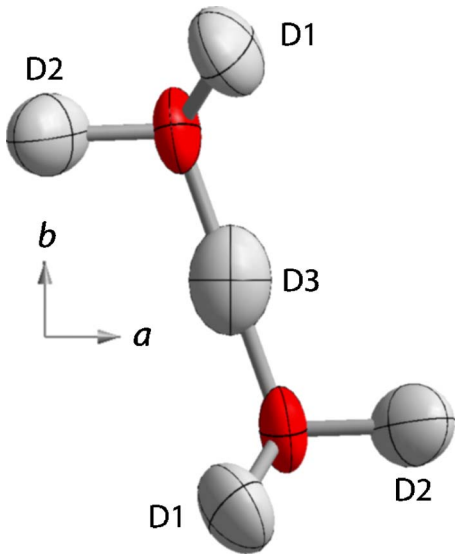

FIG. 4. (Color online) 50% probability thermal ellipsoids in the diaquahydrogen moiety determined from the 217 K HRPD data.

Upon cooling from 225 to 1.7 K, there is no significant change in the size or shape of the sulfate tetrahedron, although it shrinks by ~4% on compression to 4 kbars. The diaquahydrogen ion elongates (i.e., O2···O2 expands) by ~1% upon cooling (225–1.7 K) and ~2% upon compression (112–3950 bars). The diaquahydrogen ion in $H_5O_2^+CF_3SO_3^-$ undergoes a similar degree of expansion on cooling from 225 to 85 K.[24] The O2···O1 contact through D1 becomes longer upon cooling, while that through D2 becomes shorter. The lengthening of O2–D1···O1, when the *c* axis is shrinking, is mainly accommodated by rotation of the diaquahydrogen ions; θ changes by $-0.4(1)^\circ$ per cubic angstrom of volume decrease, whereas there is no significant change in the rotation of the sulfate ion (indicated by ω) as the volume decreases.

At all temperatures, the two hydrogen bonds, D1···O1 and D2···O1, remain 63.1(2)% and 62.9(2)% of the length of their respective O1···O2 contacts, and are not significantly different from one another. At high pressure, these hydrogen bonds become considerably more bent, and the D1–O2–D2 angle widens. Our neutron data confirm Kjällman and Olovsson's[15] inference that D3 is centered along the O2···O2 contact, forming two short, very strong, symmetrical hydrogen bonds ~1.2 Å long. These bonds are slightly bent, and the degree of bending does not change upon cooling or compression. The thermal motion of D3, and of the terminal oxygens in the $D_5O_2^+$ ion, is highly anisotropic (Fig. 4), being greatest along the long axis of the ion, although the difference tensor, $U_{ij}^{D3} - U_{ij}^{O2}$, is nearly isotropic in the *a*-*b* plane. The long axis of the D3 thermal ellipsoid makes an angle of 19(8)° with the O2···O2 vector (the uncertainty being derived from that in U_{12}). These observations are in agreement with anisotropic refinements of the diaquahydro-

TABLE IV. Parameters obtained by fitting of single- and double-Debye models to the lattice parameters of SAT-I at room pressure. For the single-Debye models (rows 1–3) the fitted parameter A is $9nk_B(\gamma/K_T)$, and for the double-Debye model is simply γ/K_T. Column 3 reports K_T/γ, although for the a and c axes we have actually given $\sqrt[3]{K_T/\gamma}$ as determined from the parameter A in column 2; this is to afford better comparison with the axial incompressibilities reported in Table V.

	x_0	A	K_T/γ (GPa)	θ_D^A (K)	θ_D^B (K)
a	7.4758(1) Å	$1.42(5)\times10^{-34}$	32.2(4)	173(20)	⋯
c	6.3255(2) Å	$1.87(2)\times10^{-33}$	13.62(5)	298(5)	⋯
V	353.52(1) Å^3	$1.17(2)\times10^{-31}$	40.4(7)	278(7)	⋯
V	353.487(8) Å^3	$7.43(2)\times10^{-11}$	13.46(4)	165[a]	956[a]

[a]Fixed.

gen ion in other compounds, and are the result of anharmonic vibration of D3 in a broad potential well coupled with librational motion of the whole ion.[25–28]

B. The thermal expansion at ambient pressure

From the data collected on POLARIS, lattice parameters at atmospheric pressure were obtained at 58 temperatures from 1.7 to 230 K, in 4 K increments, with a precision, as indicated by the Rietveld refinement standard errors of approximately three parts in 100 000. For the purpose of making a simple calculation we have fitted a third-order polynomial to the unit-cell volumes between 1.7 and 230 K (excluding the region from 160 to 190 K), $V=AT^3+BT^2+V_0$. The coefficients obtained are $A=-1.95(4)\times10^{-7}$ Å^3 K^{-3}, $B=1.53(1)\times10^{-4}$ Å^3 K^{-2}, and $V_0=353.414(5)$ Å^3 ($R^2=99.989\%$ and the maximum difference is 0.010%).

A more detailed description of the thermal expansion begins with Grüneisen's relation between the thermoelastic parameters

$$\gamma=\frac{\alpha_V V K_T}{C_V}, \tag{1}$$

where γ is the Grüneisen ratio, α_V is the volume thermal expansion coefficient, K_T is the isothermal bulk modulus, C_V is the isochoric specific heat capacity, and V the unit-cell volume. If γ and K_T are assumed to be independent of temperature, integration of Eq. (1) with respect to T leads to the following expression for the thermal expansion in terms of the internal energy of the crystal:

$$V(T)=V_0+\frac{\gamma U(T)}{K_T}, \tag{2}$$

where V_0 is the volume at 0 K. The internal energy, $U(T)$, may be obtained via a Debye approximation[29]

$$U(T)=9NK_BT\left(\frac{T}{\theta_D}\right)^3\int_0^{\theta_D/T}\frac{x^3}{e^x-1}dx, \tag{3}$$

where N is the number of atoms in the unit cell, k_B is Boltzmann's constant, θ_D is the Debye temperature, and $x=\hbar\omega/k_BT$. Note that the zero-point energy of $9Nk_B\theta_D/8$ is included in Eq. (2) via the term V_0.

In previous studies we have found that this expression or similar expressions taken to higher order[30] are capable of modeling accurately the thermal expansion of simple inorganic solids[22,31,32] over a wide temperature range, thereby providing a method of estimating both their Debye temperatures and their elastic parameters. However, in the case of molecular solids[33–36] the presence of both inter- and intramolecular vibrations means that a more realistic calculation of the internal energy, for example, using a double-Debye model fitted to experimental heat capacity data, may be required if physically sensible elastic parameters are to be extracted from $V(T)$ data. In this case, we have found that the internal energy is better represented by two Debye moments with very different characteristic temperatures, θ_D^A and θ_D^B,

$$U(T)=9nk_B\left[Xf\left(\frac{\theta_D^A}{T}\right)+Yf\left(\frac{\theta_D^B}{T}\right)\right], \tag{4}$$

where $f(\theta_D/T)$ is the Debye function, n is the number of atoms per molecule, and X and Y are mixing parameters.

The specific heat capacity of SAT was measured by Hornung and Giauque[20] in the range 15–300 K. These isochoric data were converted to isobaric values using $C_P=C_V(1+\alpha_V\gamma T)$, with α_V taken to be that measured by us for SAT and $\gamma=1$. Single- and double-Debye models were fitted to $C_V(T)$, the latter providing by far the better fit to the data. For the single-Debye model, we obtained $\theta_D=323(18)$ K, and for the double-Debye model we found $\theta_D^A=165(4)$ K and $\theta_D^B=956(6)$ K (corresponding to vibrational wavenumbers of ~115 and ~660 cm^{-1}, respectively) with $X=0.191(4)$ and $Y=0.406(15)$. As we observed in ammonia dihydrate,[32] the heat capacity does not approach the classical Dulong and Petit high-temperature limit ($3nk_B$) but instead tends toward a high-temperature limit of $\sim 2nk_B$.

Single-Debye models were used in least-squares fitting to the unit-cell edges, and to the unit-cell volume, with the respective values of θ_D freely refined. A double-Debye model, employing the two Debye temperatures obtained from the heat capacity data, was then fitted to the unit-cell volume as a function of temperature. The results of these fits are given in Table IV, and depicted in Figs. 5(a), 5(c), and 5(d). The coefficient of volume thermal expansion calculated from the double-Debye model is shown in Fig. 5(b).

The values of K_T/γ found from the single- and double-Debye fits to the unit-cell volume are 40.4(7) and 13.46(4) GPa, respectively; the latter is a much more typical value for a hydrogen-bonded crystal, and as we will show subsequently, is considerably closer to the true value (roughly 11 GPa at absolute zero).

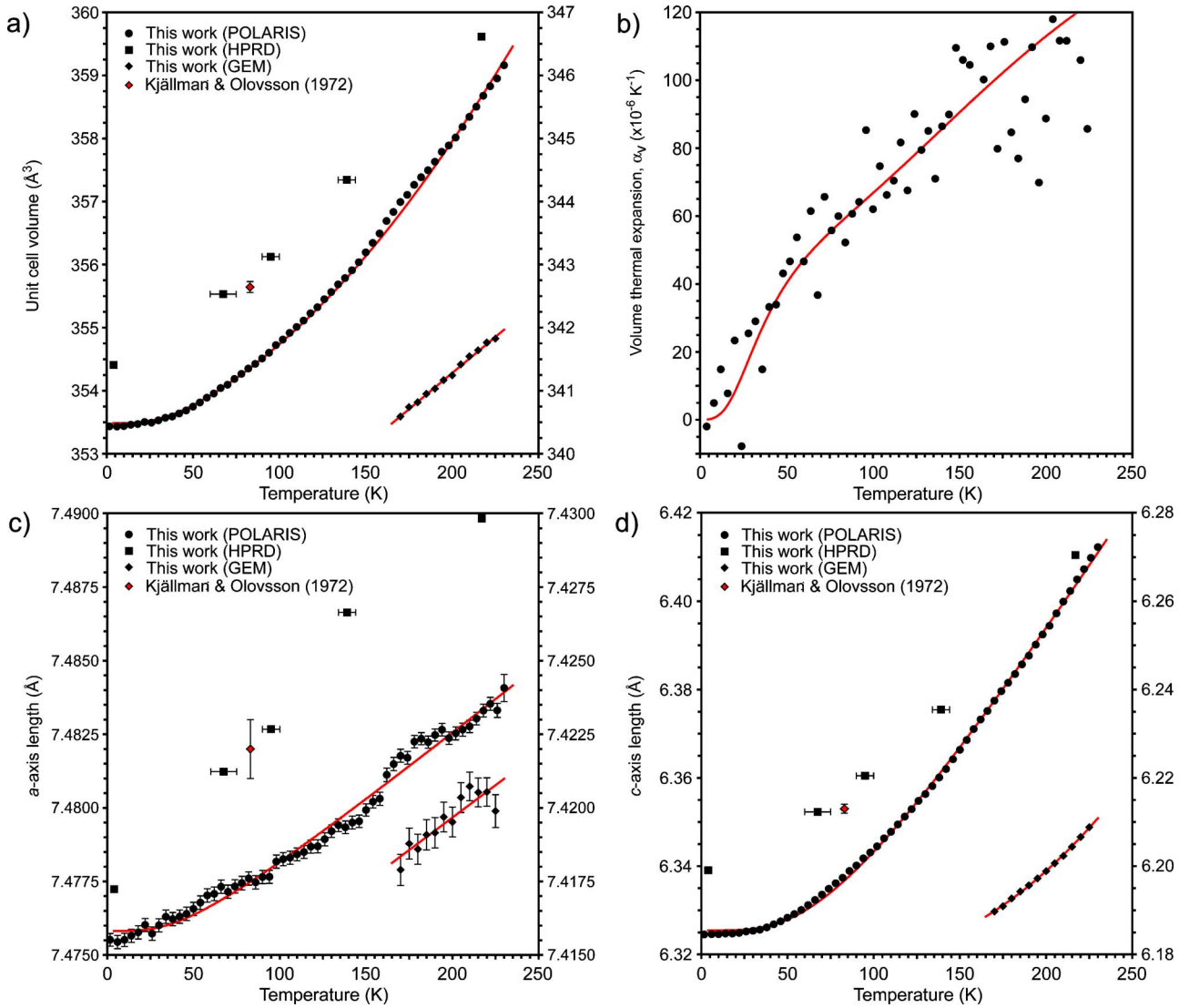

FIG. 5. (Color online) The temperature dependence of the unit-cell volume measured on POLARIS and HRPD at atmospheric pressure (read from left ordinate) and on GEM at 5.47 kbars (read from the right ordinate). The literature value is shown for comparison. The solid line through the POLARIS data is a Debye model fit to the data (with values from 162–194 K excluded), and the solid lines through the GEM data are simply linear or quadratic functions in T.

C. The thermal expansion at 5.47 kbars

Figure 5 also shows the behavior of the cell edges and the volume between 170 and 225 K at 5.47 kbars measured during the experiment using GEM: measurements were made from 50 to 225 K but much of the data had to be discarded because of a blocked pressure line (see Sec. II D). The limited data set precludes detailed analysis and the lines shown in Fig. 5 have been fitted with first- and second-order polynomials as follows: $V(T)=2.30(4)\times10^{-2}T+336.69(8)$ Å^3, $a(T)=4.5(7)\times10^{-5}T+7.411(1)$ Å, and $c(T)=1.6(2)\times10^{-6}T^2-2.9(7)\times10^{-4}T+6.193(7)$ Å.

D. The bulk and axial incompressibility

The data collected along the 200 K isotherm during compression in the TiZr pressure cell on GEM were fitted with a third-order Birch-Murnaghan equation of state,[37] which is parametrized in terms of the zero-pressure volume (V_0), zero-pressure isothermal bulk modulus ($K_{T,0}=V\partial P/\partial V$), and the first pressure derivative of the bulk modulus (K').

$$P=\frac{3}{2}K_{T,0}\left[\left(\frac{V_0}{V}\right)^{7/3}-\left(\frac{V_0}{V}\right)^{5/3}\right]\times\left[1+\frac{3}{4}(K'-4)\left(\frac{V_0}{V}\right)^{2/3}-1\right]. \quad (5)$$

Since the pressure line became blocked above 4 kbars, we discarded the data collected at 4470, 4940, and 5452 bars, and instead substituted the data point at 5470 bars, 200 K acquired during the later warming run. By defining the axial incompressibilities, K_a and K_c, as $[a^3\partial P/\partial a^3]$ and $[c^3\partial P/\partial c^3]$, respectively, they may be treated in the same way as the volume. Parameters from fitting the third order Birch-Murnaghan equation to the data are given in Table V, and the fits are shown graphically in Fig. 6.

Note that the axial incompressibilities meet the require-

TABLE V. Parameters obtained by fitting a third-order Birch-Murnaghan equation of state to data collected along the 200 K isotherm.

	Volume	a axis (a^3)	c axis (c^3)
X_0 (Å^3)	358.43(8)	419.72(14)	261.42(12)
K (GPa)	9.2(2)	18.3(10)	4.5(1)
K'	8(1)	6(4)	5.6(5)

ment (for a tetragonal crystal) that $\frac{1}{3}K^{-1}=2K_a^{-1}+K_c^{-1}$. The bulk modulus of SAT at 200 K is very close to the value for D_2O ice at the same temperature (9.18 GPa),[38] although ice is elastically isotropic whereas SAT is strongly anisotropic.

E. Pressure dependence of α_V / temperature dependence of K_T

Having determined the thermal expansivity at atmospheric pressure and at 5.5 kbars, we can estimate the pressure dependence of the thermal expansion $(\partial\alpha_V/\partial P)_T$. This is thermodynamically equivalent to the temperature dependence of the bulk modulus, $(\partial K/\partial T)_P$, the two properties being related via the isothermal Anderson-Grüneisen parameter δ_T, where

$$\delta_T=\frac{-1}{\alpha_0 K_T}\left(\frac{\partial K_T}{\partial T}\right)_P=\frac{-K_T}{\alpha_P}\left(\frac{\partial \alpha}{\partial P}\right)_T. \quad (6)$$

At 200 K 5.47 kbars we find $\alpha_P=67(1)\times10^{-6}$ K^{-1}, and at 200 K atmospheric pressure we find $\alpha_0=109(2)\times10^{-6}$ K^{-1}; using $K_T=9.2(2)$ GPa gives $(\partial K/\partial T)_P=-10.6(5)$ MPa K^{-1}. For comparison, a quadratic fit to the bulk modulus of D_2O ice[38] over the same temperature range yields $(\partial K/\partial T)_P=-11.0(2)$ MPa K^{-1} at 200 K.

F. The high-pressure phase SAT-II

Warming of the low-pressure phase SAT-I along the 5.5 kbar isobar resulted in the formation of a new phase (SAT-II) above 230 K. The diffraction pattern of SAT-II collected at 235 K, 5455 bars was indexed using DICVOL04 (Ref. 39) with a monoclinic unit cell and figures of merit, $M(14)=37.6$ and $F(14)=45.8$ [0.0118, 26];[40,41] subsequent LeBail profile refinements using GSAS gave the cell dimensions listed in Table VI. Attempts to solve the structure of SAT-II using the GEM data have not been successful, most likely because of strong preferred orientation. However, we were able to quench SAT-II within the stability field of SAT-I, and the data collected allow us to estimate the bulk thermoelastic properties; these yield insights into the likely molecular arrangement of the high-pressure phase.

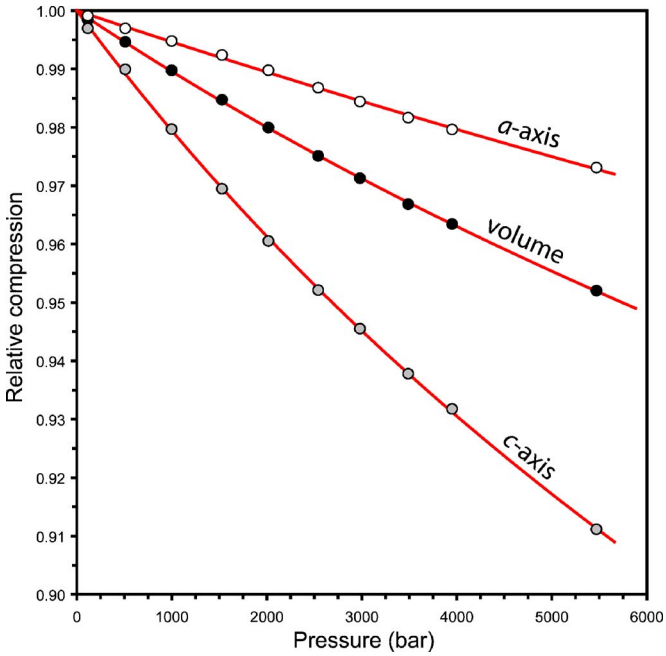

FIG. 6. (Color online) The relative incompressibility of the volume and of the a and c axes of SAT at 200 K. Solid lines are third-order Birch-Murnaghan fits with parameters reported in Table IV.

The unit cell volume of SAT-II at 235 K, 5.5 kbars is ~6.7% *less* dense than SAT-I at 225 K, 5.5 kbars; contrast this with the orthorhombic high-T form of selenic acid tetrahydrate,[42] which is denser than the tetragonal form (isomorphous with SAT-I), and consists of a mixture of hexagonal and pentagonal oxygen rings.

A second-order polynomial fitted to the three data points along the 5.5 kbar isobar allows us to make an estimate of the thermal expansivity of SAT-II as a function of temperature; at 200 K, the coefficients of volume and axial thermal expansion are $\alpha_V\approx102\ \mu$K^{-1}, $\alpha_{a\sin\beta}\approx30\ \mu$K^{-1}, $\alpha_b\approx26\ \mu$K^{-1}, and $\alpha_c\approx46\ \mu$K^{-1}. This value of α_V is ~40% larger than the value for SAT-I at the same pressure and temperature.

Similarly, we can obtain rough estimates of the incompressibility of SAT-II along the 200 and 50 K isotherms using the values in columns 2 and 5, and columns 3 and 4, respectively, of Table VI. The bulk and axial elastic moduli at 200 K are $K_{200,2750}\approx19.1$ GPa, $K_{a\sin\beta}\approx18.8$ GPa, $K_b\approx18.1$ GPa, and $K_c\approx20.6$ GPa, and at 50 K are $K_{50,0}\approx17.7$ GPa, $K_{a\sin\beta}\approx18.2$ GPa, $K_b\approx15.6$ GPa, and $K_c\approx19.7$ GPa. Very approximately, these results indicate a

TABLE VI. Unit-cell dimensions of SAT-II obtained by LeBail profile refinement of GEM bank 4 diffraction patterns.

	235 K 5455 bar	200 K 5450 bar	50 K 5435 bar	70 K 125 bar	205 K 2750 bar
a (Å)	6.1902(3)	6.1819(4)	6.1594(2)	6.2220(4)	6.2188(7)
b (Å)	11.1234(5)	11.1123(7)	11.0853(4)	11.1962(7)	11.1782(10)
c (Å)	5.6446(3)	5.6347(4)	5.6134(3)	5.6627(4)	5.6612(7)
β	110.287(4)°	110.252(5)°	110.229(3)°	110.316(5)°	110.387(5)°
V (Å^3)	364.56(2)	363.15(3)	359.64(2)	369.94(3)	368.89(9)

value for $(\partial K/\partial T) \approx -9.3$ MPa K^{-1}, which is similar to that found in SAT-I. However, SAT-II is more elastically isotropic than SAT-I, where the axial incompressibility along the *c* axis is three times smaller than along the other two orthogonal directions. The axial moduli of SAT-II are very similar to the *a*-axis incompressibility of SAT-I, perhaps suggesting that the hydrogen-bonding pattern in the *a*-*b* plane of SAT-I occurs in SAT-II as a three dimensional network. It is intriguing that SAT-II has a higher bulk modulus *and* a larger thermal expansivity than SAT-I; typically one would expect the more incompressible structure to have a smaller expansivity.

IV. SUMMARY

Our powder neutron diffraction data have revealed the highly anisotropic thermoelastic behavior of perdeuterated sulfuric acid tetrahydrate. Approaching the melting point (232 K), approximately 80% of the thermal expansion is along the *c* axis, and at 200 K the *c* axis is roughly four times more compressible than the *a* axis. This anisotropy occurs because of the orientation of the very stiff diaquahydrogen ions in the *a*-*b* plane. The bonding in the *a*-*b* plane is characterized by orthogonal chains of weak hydrogen bonds (D2···O1) alternating with very strong hydrogen bonds (O2···D3···O2), whereas the bonding along the *c* axis is solely through the weak D1···O1 hydrogen bond. In contrast, the newly discovered high-pressure polymorph, SAT-II, is nearly elastically isotropic, and we predict that the structure is characterized by a three dimensional network of weak and strong hydrogen bonds.

ACKNOWLEDGMENTS

The authors wish to thank the ISIS facility for beam time, and Andy Church, Chris Goodway, and Jon Bones for technical support. This work is supported by PPARC Grant Nos. PPA/P/S/2003/00247 and PP/E006515/1.

[1] K. D. Beyer, A. R. Hansen, and M. Poston, J. Phys. Chem. A **107**, 2025 (2003).
[2] D. R. Allan, S. J. Clark, A. Dawson, P. A. McGregor, and S. Parsons, J. Chem. Soc. Dalton Trans. **2002**, 1867 (2002).
[3] F. P. A. Fabbiani, D. R. Allan, D. J. Francis, W. G. Marshall, and C. R. Pulham, Inorg. Chim. Acta **361(2)**, 487 (2008).
[4] R. Zhang, P. J. Wooldridge, J. P. D. Abbatt, and M. J. Molina, J. Phys. Chem. **97**, 7351 (1993).
[5] A. K. Bertram, D. D. Patterson, and J. J. Sloan, J. Phys. Chem. **100**, 2376 (1996).
[6] T. J. Fortin, K. Drdla, L. T. Iraci, and M. A. Talbert, Atmos. Chem. Phys. **3**, 987 (2003).
[7] E. Girard, J. P. Blanchet, and Y. Dubois, Atmos. Res. **73**, 131 (2005).
[8] T. B. McCord, G. B. Hansen, D. L. Matson, T. V. Johnson, J. K. Crowley, F. P. Fanale, R. W. Carlson, W. D. Smythe, P. D. Martin, C. A. Hibbitts, J. C. Granahan, A. Ocampo, and the NIMS Team, J. Geophys. Res., [Planets] **104**, 11827 (1999).
[9] T. B. McCord, G. B. Hansen, and C. A. Hibbitts, Science **292**, 1523 (2001).
[10] J. B. Dalton III, O. Prieto-Ballesteros, J. S. Kargel, C. S. Jamieson, J. Jolivet, and R. Quinn, Icarus **177**, 472 (2005).
[11] J. S. Kargel, J. Z. Kaye, J. W. Head, G. M. Marion, R. Sassen, J. K. Crowley, O. Prieto-Ballesteros, S. A. Grant, and D. L. Hogenboom, Icarus **148**, 226 (2000).
[12] T. M. Orlando, T. B. McCord, and G. A. Grieves, Icarus **177**, 528 (2005).
[13] R. W. Carlson, M. S. Anderson, R. Mehlman, and R. E. Johnson, Icarus **177**, 461 (2005).
[14] A. D. Fortes, I. G. Wood, and K. S. Knight, J. Chem. Phys. **125**, 144510 (2006).
[15] T. Kjällman and I. Olovsson, Acta Crystallogr., Sect. B: Struct. Crystallogr. Cryst. Chem. **28**, 1692 (1972).
[16] J. L. Finney, Acta Crystallogr., Sect. B: Struct. Sci. **51**, 447 (1995).
[17] S. Hull, R. I. Smith, W. I. F. David, A. C. Hannon, J. Mayers, and R. Cywinski, Physica B **180 & 181**, 1000 (1992).
[18] A. C. Hannon, Nucl. Instrum. Methods Phys. Res. A **551**, 88 (2005).
[19] R. M. Ibberson, W. I. F. David, and K. S. Knight, *The High Resolution Neutron Powder Diffractometer (HRPD) at ISIS—A User Guide* (Rutherford Appleton Laboratory, Oxfordshire, UK 1992) RAL-92-031. (http://www.isis.rl.ac.uk/crystallography/documentation/HRPDguide)
[20] E. W. Hornung and W. F. Giauque, J. Am. Chem. Soc. **77**, 2983 (1955).
[21] A. C. Larsen and R. B. Von Dreele, General Structure Analysis System (GSAS), Los Alamos National Laboratory Report No. LAUR 86-748, Los Alamos, NM, 2000 (http://www.ncnr.nist.gov/xtal/software/gsas.html).
[22] I. G. Wood, L. Vočadlo, K. S. Knight, D. P. Dobson, W. G. Marshall, G. D. Price, and J. P. Brodholt, J. Appl. Crystallogr. **37**, 82 (2004).
[23] L. Vočadlo, J. Brodholt, D. Dobson, K. S. Knight, W. G. Marshall, G. D. Price, and I. G. Wood, Earth Planet. Sci. Lett. **203**, 567 (2002).
[24] R. G. Delapane, J.-O. Lundgren, and I. Olovsson, Acta Crystallogr., Sect. B: Struct. Crystallogr. Cryst. Chem. **31**, 2202 (1975).
[25] A. Sequeira, C. A. Berkebile, and W. C. Hamilton, J. Mol. Struct. **1**, 283 (1967).
[26] A. L. MacDonald, J. C. Speakman, and D. Hadži, J. Chem. Soc., Perkin Trans. 2 **1972**, 825.
[27] J. Roziere and J. M. Williams, Inorg. Chem. **15**, 1174 (1976).
[28] R. Attig and J. M. Williams, J. Chem. Phys. **66**, 1389 (1977).
[29] W. Cochran, *The Dynamics of Atoms in Crystals* (Arnold, London, 1973).
[30] D. C. Wallace, *Thermodynamics of Crystals* (Dover, New York, 1998).
[31] L. Vočadlo, K. S. Knight, G. D. Price, and I. G. Wood, Phys. Chem. Miner. **29**, 132 (2002).
[32] I. G. Wood, K. S. Knight, G. D. Price, and J. A. Stuart, J. Appl. Crystallogr. **35**, 291 (2002).
[33] A. D. Fortes, I. G. Wood, K. S. Knight, J. P. Brodholt, M. Alfredsson, G. S. McGrady, and L. Vočadlo, J. Chem. Phys. **119**, 10806 (2003).
[34] A. D. Fortes, I. G. Wood, K. S. Knight, M. Alfredsson, and L. Vočadlo, J. Appl. Crystallogr. **38**, 612 (2005).
[35] A. D. Fortes, I. G. Wood, M. Alfredsson, L. Vočadlo, and K. S. Knight, Eur. J. Mineral. **18**, 449 (2006).
[36] A. D. Fortes, I. G. Wood, L. Vočadlo, H. E. A. Brand, and K. S. Knight, J. Appl. Crystallogr. **40**, 761 (2007).
[37] F. Birch, J. Geophys. Res. **57**, 227 (1952).
[38] U. Mitzdorf and D. Helmreich, J. Acoust. Soc. Am. **49**, 723 (1971).
[39] A. Boultif and D. Louër, J. Appl. Crystallogr. **37**, 724 (2004).
[40] P. M. De Wolff, J. Appl. Crystallogr. **5**, 108 (1968).
[41] G. S. Smith and R. L. Snyder, J. Appl. Crystallogr. **12**, 60 (1979).
[42] T. Dahlems and D. Mootz, Z. Anorg. Allg. Chem. **622**, 1319 (1996).